# A new, global, multi-annual (2000–2007) burnt area product at 1 km resolution

Kevin Tansey,[1] Jean-Marie Grégoire,[2] Pierre Defourny,[3] Roland Leigh,[1] Jean-François Pekel,[3] Eric van Bogaert,[3] and Etienne Bartholomé[2]

Received 2 August 2007; revised 8 October 2007; accepted 20 November 2007; published 1 January 2008.

[1] This paper reports on the development and validation of a new, global, burnt area product. Burnt areas are reported at a resolution of 1 km for seven fire years (2000 to 2007). A modified version of a Global Burnt Area (GBA) 2000 algorithm is used to compute global burnt area. The total area burnt each year (2000–2007) is estimated to be between 3.5 million km$^2$ and 4.5 million km$^2$. The total amount of vegetation burnt by cover type according to the Global Land Cover (GLC) 2000 product is reported. Validation was undertaken using 72 Landsat TM scenes was undertaken. Correlation statistics between estimated burnt areas are reported for major vegetation types. The accuracy of this new global data set depends on vegetation type. **Citation:** Tansey, K., J.-M. Grégoire, P. Defourny, R. Leigh, J.-F. Pekel, E. van Bogaert, and E. Bartholomé (2008), A new, global, multi-annual (2000–2007) burnt area product at 1 km resolution, *Geophys. Res. Lett.*, *35*, L01401, doi:10.1029/2007GL031567.

## 1. Introduction

[2] Global burnt area products are in high demand from research groups and communities interested in climate, atmospheric emissions, carbon cycling and pollution resulting from fires and the impact of vegetation burning on land cover change [*Patra et al.*, 2005; *Jupp et al.*, 2006]. Burnt area is a crucial component in the computation of gas emissions [*Seiler and Crutzen*, 1980]. Currently, global burnt area products have been limited in time. As its name suggests, the GBA2000 product [see *Tansey et al.*, 2004] was limited to the year 2000. This was also true of the European Space Agency (ESA) GlobScar product [*Simon et al.*, 2004]. ESA have recently released their GLOBCARBON burnt area product (http://geofront.vgt.vito.be/) covering the period 1998–2007 and MODIS burnt area products have started to be made available for public use [*Roy et al.*, 2005]. Multi-annual products are needed to strengthen the understanding of relationships between vegetation, climate and fire.

[3] A number of papers have reported burnt area estimates using active fire data as a proxy. *Schultz* [2002] used ATSR fire count data; *Sukhinin et al.* [2004] used AVHRR data; *Giglio et al.* [2006] and *Smith et al.* [2007] used MODIS active fire data. These authors highlight the lack of accurate, consistent long-term information on global burnt area as the reason for their decision to use active fire data. Recently, *Turquety et al.* [2007] used fire perimeter data with large uncertainties (of the order of 50%) with active fire data to derive emissions from boreal forest fires. *Stohl et al.* [2006] in their assertion that record high air pollution was caused by agricultural fires in Eastern Europe assumed that every MODIS active fire detected resulted in a burnt area of 180 hectares. Their assumption was derived from a statistical analysis of boreal forest fires presented by *Wotawa et al.* [2006]. Our observations indicate that the characteristics of burning activity (size of fire, intensity of fire, number of fires) in agricultural and forest areas differ greatly. The uncertainties associated with using active fires as a proxy for burnt area are described by *van der Werf et al.* [2006]. We have made available to the scientific community a long-term (covering seven global fire seasons between 2000 and 2007), moderate spatial resolution (1 km$^2$), high temporal resolution global burnt area product derived from direct observations from the SPOT VEGETATION sensor. Furthermore, the product has been evaluated against a large number of Landsat TM images and a number of regional products derived from in situ or remote means. We evaluate the product in its ability to correctly quantify the amount of burnt area by computing comparative values over a global hexagonal grid with a cell spacing of 60 km. This is done over a number of different vegetation types. We acknowledge that the classification of Landsat TM to burnt area and a comparison with our product is not a complete validation of the results. The implications of the validation are discussed later. To differentiate this product from others that have been produced before or are in development, this product will be referred to as the L3JRC (pronounced L-three-J-R-C) product.

## 2. Methodology

[4] A single algorithm is used to classify burnt areas from SPOT VEGETATION reflectance data. SPOT 4 was launched in 1998 into a polar sun synchronous orbit at 832 km. The revisit period of the VEGETATION instrument is around five days. The burnt area algorithm was developed by D. Ershov and colleagues under contract to the Joint Research Centre of the European Commission in the GBA2000 project [*Tansey et al.*, 2004]. The algorithm was used successfully over a wide geographical area, on a number of different vegetation types, in the GBA2000 product and it was felt that it could be adapted for application at the global scale. It has subsequently been modified by the authors. Global, daily, atmospheric corrected (using Simplified Method for Atmospheric Correc-

[1]Department of Geography, University of Leicester, Leicester, UK.
[2]Joint Research Centre of the European Commission, Ispra, Italy.
[3]ENGE Unité Environnemétrie et Géomatique, Université Catholique de Louvain, Louvain-la-Neuve, Belgium.


0094-8276/08/2007GL031567$05.00

tion (SMAC) code [see *Rahman and Dedieu*, 1994]) S1 data were used as input. In the pre-processing module, cloud and snow masks are generated based on thresholds at 0.45 $\mu$m and 1.66 $\mu$m (SWIR) wavelengths. We restrict observations of the ground to satellite view zenith angles of less than 50.5 degrees. A fire smoke mask is generated using thresholds at 0.45 $\mu$m. A cloud shadow mask is derived using solar and view azimuth and zenith angles and assuming a constant cloud height of 10 km. This will normally result in an over compensation of the mask to be confident that all cloud shadows are removed. A binary mask is then derived of all pixels that appear saturated in the 1.66 $\mu$m channel. A sun shadow mask is produced from the GTOPO 30 global DEM. We compute aspect and slope and use a threshold that assumes a pixel will be in the shade if the sun incidence angle is above 75 degrees. An evaluation of this mask shows that only very mountainous regions of the world are masked during winter seasons. These masks are combined to create a contaminated pixel product that is computed on a daily basis for the global data set. The main processing algorithm makes use of a temporal index in the 0.83 $\mu$m (near infrared, NIR) channel. This index I is computed using the following method:

$$I = \frac{S1_{NIR} - IC_{NIR}}{S1_{NIR} + IC_{NIR}} \quad (1)$$

where $S1_{NIR}$ is the pixel value of the S1 daily product and $IC_{NIR}$ an intermediate composite product. The intermediate composite consists of averaged NIR reflectances derived from all observations prior to observation on the day being considered. No calculation or detection is performed where $S1_{NIR}$ or $IC_{NIR}$ equals zero. Mean and standard deviation values are computed for the index I over a window of 200 by 200 pixels ignoring all pixels with a value of zero or identified as being contaminated. A pixel is flagged as burnt if the pixel value in the 200 by 200 pixel array, I, is lower than the mean value minus two standard deviations. Two further checks are made on reflectance values in the 0.83 $\mu$m (S1 pixel value < 260) and 1.66 $\mu$m (S1 pixel value > 250) channels to confirm the burnt area. To compute the updated intermediate composite in the near infrared channel ($IC_{NIR}$), we first calculate a phase value that uses sun and viewing angles (both zenith and azimuth) to evaluate the suitability of a pixel to be used in future composites. If this test is passed, then the new value of the composite is the average between the existing composite value and the pixel value of the S1 product being analyzed. Post-processing of the data serves to utilize the latest land cover information to remove some over detections believed mainly to be due to some shadowing not excluded with the relief/sun shadow mask, the multi-annual detection of leaf off conditions in temperate regions and lake melt conditions at high northern latitudes. The GLC2000 land cover product was used (Global Land Cover 2000 database, European Commission, Joint Research Centre, 2003, http://www-gem.jrc.it/glc2000) to provide updated information on water bodies, snow and ice, bare surfaces and urban areas. We used the 'sparse herbaceous or sparse shrub cover' class of GLC2000 to remove detections made at latitudes greater than 60°N. In latitudes greater than 27°N and 27°S, we analyzed the occurrence on multiple detections of burnt area over an initial data set of four fire seasons (2000–01 to 2003–04). After an in-depth visual analysis, we assume that only those areas associated with some kind of agricultural activity were likely to burn in at least three fire seasons. This is based on the time taken for natural vegetation at temperate latitudes to grow back to a state that it could burn again being longer than three years. We used three classes in GLC2000 that identify cropland either alone or with other vegetation to remove multiple (at least three out of four) detections outside of these regions. These three post-processing steps removed approximately 14% of the total number of pixels identified as being burnt across the four fire seasons – 2000–01 to 2003–04. For the detailed analysis of burnt area, the maps were re-projected into Goodes Interrupted Homolosine with a pixel spacing of 1 km.

## 3. Results

[5] Estimates of burnt area over seven fire years are shown in Table 1. These values are reported for sixteen vegetation types from the GLC2000 product. The classes '10- tree cover, burnt', '7- tree cover, regularly flooded, fresh water' and '8- tree cover, regularly flooded, saline water' are not shown. A fire year starts on the 1st April of any year and finishes the following year on the 31st March. We assume that a fire only occurs once during any fire year.

[6] The variation in global annual burnt area is shown in Table 1. It shows that global burnt area estimates exceeded four million km$^2$ in fire years 2001–02, 2003–04 and 2006–07. It shows that there is a difference of almost one million km$^2$ between the year with the greatest amount of burnt area detected (2006–07) and the year with the least amount detected (2002–03). Comparison is made with values reported in the Global Fire Emissions Database (GFED) v2 [*van der Werf et al.*, 2006] database and with the GBA2000 project [*Tansey et al.*, 2004].

[7] The ability of the L3JRC product to estimate burnt area within a specified area has been determined. A hexagonal reference grid similar to that used by *Boschetti et al.* [2004] was reproduced for this validation. The grid resolution can be adjusted within certain limitations to the desired scale; in this case hexagons were approximately 60 km apart with an area of about 3000 km. This resolution was identical to that used by *Boschetti et al.* [2004] and was considered appropriate for this analysis while remaining computationally feasible. The exact location of the hexagons is determined by the use of an initial icosahedron [*Fuller*, 1975], ensuring that none of the 12 pentagonal intersections are located over land. Each triangular face of the icosahedron is then subdivided into hexagons using an aperture three subdivision [*Sahr and White*, 1998]. Each hexagon then subdivides into seven smaller hexagons in each iteration.

[8] 72 reference data sets derived from Landsat TM images were acquired. They were geographically spaced to include 14 in Africa (Botswana, Mozambique, Central African Republic, South Africa, Sudan, Zambia, Burkina Faso, Democratic Republic of Congo, Sudan, Zimbabwe, Algeria and Mali), 12 in Europe, Turkey and Russia (Portugal, Spain, France, Greece and Bulgaria), 13 in Australia, 14 in South America (Brazil, Paraguay and Argentina) and 19 in the USA and Canada. A full description of each reference data set is given on the project web

**Table 1.** Global Burnt Area Estimates ($km^2$) Segregated by GLC2000 Vegetation Cover Type for the 7 Fire Years From 2000 to 2007[a]

| | Fire Years | | | | | | |
|---|---|---|---|---|---|---|---|
| | 2000–01 | 2001–02 | 2002–03 | 2003–04 | 2004–05 | 2005–06 | 2006–07 |
| GLC2000 class number and name[b] | | | | | | | |
| 1 Tree cover, broadleaved, evergreen | 63349 | 73624 | 77815 | 76399 | 64647 | 59956 | 81969 |
| 2 Tree cover, broadleaved, deciduous, closed | 326989 | 360206 | 256983 | 412314 | 354088 | 326485 | 426133 |
| 3 Tree cover, broadleaved, deciduous, open | 651694 | 648824 | 593106 | 613659 | 541624 | 506167 | 631804 |
| 4 Tree cover, needle leaved, evergreen | 132461 | 160679 | 126169 | 217799 | 162670 | 158051 | 216127 |
| 5 Tree cover, needle leaved, deciduous | 109962 | 149581 | 102160 | 249301 | 151326 | 211374 | 219782 |
| 6 Tree cover, mixed leaf type | 51546 | 73625 | 35463 | 104255 | 74559 | 77573 | 93425 |
| 9 Mosaic: tree cover and other natural vegetation | 113306 | 96711 | 91004 | 98948 | 94951 | 96378 | 122821 |
| 11 Shrub cover, closed-open, evergreen | 26268 | 32036 | 20578 | 39201 | 32639 | 32766 | 38248 |
| 12 Shrub cover, closed-open, deciduous | 812915 | 846913 | 695324 | 771446 | 714878 | 621649 | 796768 |
| 13 Herbaceous cover, closed-open | 416054 | 433457 | 358087 | 420996 | 361473 | 317497 | 421776 |
| 14 Sparse herbaceous cover or sparse shrub cover | 307593 | 403032 | 351581 | 326196 | 306265 | 279891 | 367780 |
| 15 Regularly flooded shrub or herbaceous cover | 51371 | 59224 | 48861 | 72749 | 66759 | 61621 | 78843 |
| 16 Cultivated and managed areas | 537681 | 654267 | 516119 | 654955 | 590889 | 533891 | 647144 |
| 17 Mosaic: crop land, tree cover and other natural vegetation | 38413 | 43568 | 33295 | 42428 | 39071 | 37540 | 48098 |
| 18 Mosaic: crop land, shrub and grass cover | 172785 | 189254 | 154229 | 219245 | 177098 | 186459 | 211896 |
| Total, $km^2$ | 3812387 | 4225001 | 3460774 | 4319891 | 3732937 | 3507298 | 4402614 |
| Calendar years | 2000 | 2001 | 2002 | 2003 | 2004 | 2005 | 2006 |
| GFED (note that calendar year totals are shown) | 3580000 | 3742000 | 3510000 | 2966000 | 3193000 | - | - |
| GBA2000 (note that calendar year totals are shown) | 3500000 | - | - | - | - | - | - |

[a]A fire year is defined as the period from 1st April to 31st March. Comparison values for the Global Fire Emissions Database (GFED) v2 [*van der Werf et al.*, 2006] and GBA2000 [*Tansey et al.*, 2004] products are shown.

[b]GLC2000 classes 7 (Tree cover, regularly flooded, fresh water), 8 (Tree cover, regularly flooded, saline water) and 10 (Tree cover, burnt) are not shown in this table.

page provided in the next paragraph. For each reference data set, an image pair was used and a start date and end date for the validation specified. The reference data were received from the European Space Agency and independently verified by the authors. The available Landsat TM reference data were mostly from the year 2000. The spatial resolution of the data sets used for validation was approximately 30 m. However, when Landsat quicklooks were used to verify burnt area, the resolution was downgraded to 300 m. The percentage of the area of each hexagon detected as being burnt was computed for the reference and the L3JRC product.

[9] For each reference site, maps of burnt area detected by L3JRC and Landsat TM are available at http://www-tem.jrc.it/Disturbance_by_fire/products/burnt_areas/index.htm. These maps are very useful to visualize the correspondence between the data sets. Summaries of the product's accuracy arranged by continent are also provided

**Table 2.** Number of Validation Hexes, Regression Slope, Regression Intercept and Standard Deviation of Burnt Area Using the L3JRC Algorithm in Comparison With Landsat Burnt Area for Dominant Vegetation Cover Type[a]

| GLC2000 Class Number and Name[b] | Hexes | Regression Slope | Regression Intercept | St. Dev. |
|---|---|---|---|---|
| 1 Tree cover, broadleaved, evergreen | 31 | 0.4065 | −0.2739 | 4.5640 |
| 2 Tree cover, broadleaved, deciduous, closed | 10 | 0.4908 | 1.001 | 1.8998 |
| 3 Tree cover, broadleaved, deciduous, open | 36 | 0.5484 | 1.8676 | 7.1491 |
| 4 Tree cover, needle leaved, evergreen | 50 | 0.5000 | 0.6176 | 1.6937 |
| 5 Tree cover, needle leaved, deciduous | 18 | 1.3222 | 0.3558 | 3.0265 |
| 9 Mosaic: tree cover and other natural vegetation | 9 | 0.0352 | 0.9379 | 0.5653 |
| 12 Shrub cover, closed-open, deciduous | 140 | 0.5424 | 1.0973 | 6.2156 |
| 13 Herbaceous cover, closed-open | 47 | 0.1004 | 0.6208 | 1.4902 |
| 14 Sparse herbaceous cover or sparse shrub cover | 67 | 0.0454 | 0.7426 | 3.1765 |
| 15 Regularly flooded shrub or herbaceous cover | 8 | 0.5587 | 0.0732 | 1.3570 |
| 16 Cultivated and managed areas | 31 | 0.3911 | 0.7740 | 2.4610 |
| 18 Mosaic: crop land, shrub and grass cover | 6 | 0.4741 | −2.0596 | 1.8980 |

[a]The L3JRC burnt area estimate is the dependent variable.
[b]GLC2000 classes 6 (Tree cover, mixed leaf type), 11 (Shrub cover, closed-open, evergreen) and 17 (Mosaic: cropland/tree cover/other natural vegetation) are not shown as the number of hexagons for validation are equal to or less than five.

on the web page given above. In this paper we summarize the performance of the algorithm to quantify burnt area within 12 vegetation cover types described by the GLC2000 product. The dominant land cover type represented in each hexagon has been determined. Table 2 shows the number of hexagons used to validate the burnt area estimates within each hexagon and represented by the dominant land cover type. When compared to Table 1, three classes (6- tree

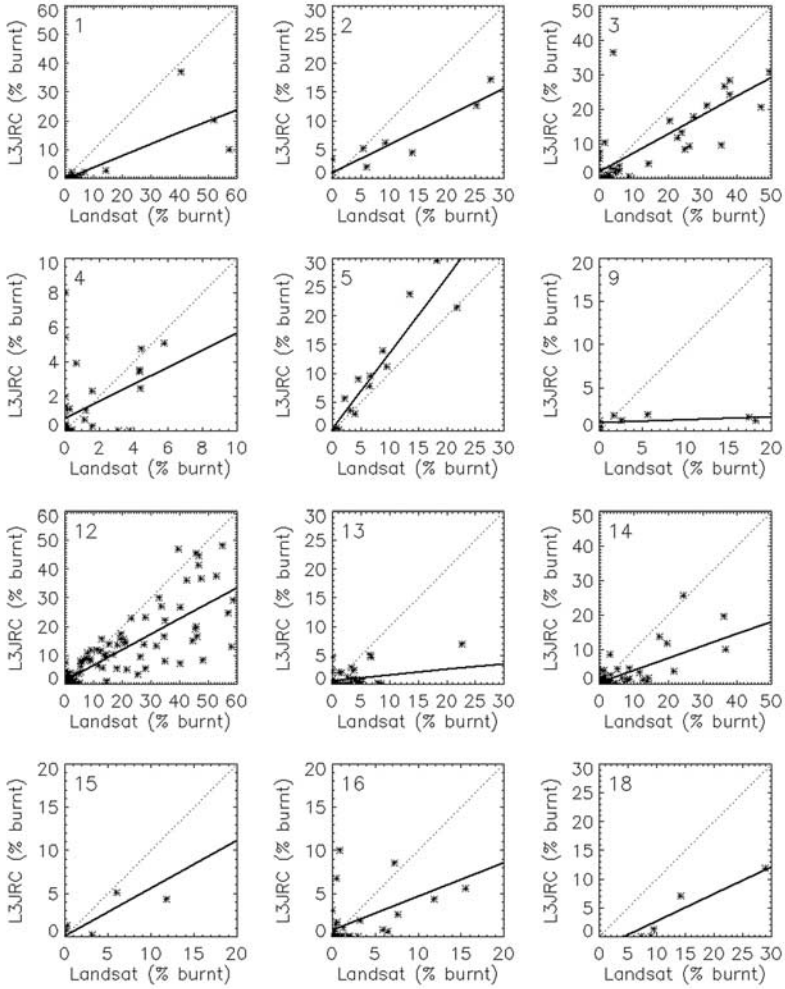


**Figure 1.** Correlation plots of burnt area detected by the L3JRC algorithm (y-axis) and derived from Landsat TM (x-axis) products (and other sources) for 12 vegetation types. The GLC2000 land cover class number is given in the upper left corner of each plot; refer to Table 1 for a description of each class. Each point corresponds to a hexagon.

**Table 3.** Number of Validation Hexes, Regression Slope, Regression Intercept and Standard Deviation of Burnt Area Using the L3JRC Algorithm in Comparison With Landsat Burnt Area for Continental Region[a]

| Region | Hexes | Regression Slope | Regression Intercept | St. Dev. |
|---|---|---|---|---|
| Europe and northern Asia | 66 | 0.9768 | 0.1195 | 2.6992 |
| North America | 106 | 0.4257 | 0.9258 | 2.0578 |
| South America | 85 | 0.5537 | −0.1782 | 1.9054 |
| Southern Asia, Gulf States and Australia | 121 | 0.4635 | 1.0386 | 6.6135 |
| Africa and Middle East | 76 | 0.5434 | 0.4580 | 6.8940 |

[a]The L3JRC burnt area estimate is the dependent variable. A description of the geographical location of each region is given in the text.

cover, mixed leaf type, 11- shrub cover, closed-open, evergreen and 17- mosaic: cropland/tree cover/other natural vegetation) are not shown as the number of hexagons are equal to or less than three. The relationship between burnt area mapped from L3JRC and Landsat TM is shown in Figure 1 for the vegetation cover types described in Table 2.

[10] The performance of the algorithm on a continental scale is shown in Table 3. Europe and northern Asia is a box ending at 35 N, North America includes parts of Central America ending at 15 N, South America is below this line, Africa includes parts of the Middle East up to 35 N and 50 East, Southern Asia and Australia is below 35 N and 50 E.

## 4. Discussion and Implications

[11] Any effort to characterize burnt area using a single algorithm must be able to detect changes in reflectance that are caused by fires of varying intensity and size that occur in different vegetation types including grassland, forest and croplands. The validation results indicate that the L3JRC algorithm performs reasonably well in a number of different vegetation types. If we use the standard deviation as an indicator of accuracy (not bias), we can report standard deviations away from the best fit line of between 0.5 and 7% (Table 2). However, the algorithm performs poorly in areas of low vegetation cover (GLC2000 classes 13 (herbaceous cover) and 14 (sparse herbaceous or shrub cover) where there is a significant underestimation in the amount of burnt area. A more detailed investigation into this observation revealed that very little evidence of a burn scar could be seen when limited to visible and near infrared wavelengths of SPOT VEGETATION. Very low intensity fires in sparse vegetation revealed only a subtle change at middle infrared wavelengths. These types of burnt area are seen in semi-arid Australia and Africa. The amount of burnt area detected by the L3JRC algorithm for all vegetation types reported in Table 2 is, on average, less than the amount detected by Landsat TM. We will obviously miss small burnt areas (nominally <50 hectares) and exclude detail at the boundary of the burnt area. This under detection by L3JRC seems to be more significant in areas of shrubs and grasses rather than forests. As the original algorithm was developed for detection of burnt area in boreal forest, this might be expected. The result of the validation over cultivated and managed areas seems to indicate that the L3JRC algorithm misses many burnt areas. It is likely that the physical size of burn scars in cultivated areas may be too small for detection by SPOT VEGETATION. This will be investigated in the future with the use of active fire information. It is noted that many agricultural fires are detected in southern Russia, South America, United States and in Australia. It is hypothesized here that the true scale of burning activity in agricultural areas is much greater than the scale reported in this paper and therefore quantification of this area must be a topic of future research. The accuracy of the continental products (Table 3) also tells us that there are consistent under estimations in burnt area estimations, with the exception of Europe and northern Asia. Potential improvements in the algorithm will include an investigation into improving detection success in shrubs, grasses and sparsely vegetated surfaces if it is determined that the burn scar is large enough to be detected. The burnt area estimates reported for L3JRC for the fire year 2000–01 of 3.81 million km$^2$ are in-line with estimates reported in the original GBA2000 product for the calendar year 2000 of approximately 3.5 million km$^2$ [*Tansey et al.*, 2004]. Burnt areas reported by *van der Werf et al.* [2006] are also of the same order (apart from in 2003) as L3JRC results assuming that the disparity between reporting by fire year and calendar year does not result in a significant difference in the amount of vegetation burnt. This is a reasonable assumption to make given that the majority of fires that occur in the first three months of the year do so in sub-Saharan Africa and occur in most years.

[12] The validation exercise tells the user the likelihood that the amount of burnt area within a specified area and over a certain time period is correctly detected. The time period over which the products are evaluated ranges between three and nine months. The day-to-day accuracy of burnt area detection is not reported. The validation results do not tell us the whether the burn scars are spatially or temporally correlated in any quantitative method (a qualitative indication can be seen in plots on the L3JRC web site). However, we believe that users will be interested in the performance of the algorithm over a time period of several weeks or the full fire season. When using individual daily products, it should be noted that a successful detection of a burnt area can only be made if a clear observation of the surface is made. This might not for a number of days after a fire has occurred. Therefore, the product is not a robust indicator that a fire has occurred on a given day. The advantage of the daily product is that it can be assimilated over a specific time period to suite other experiments and observations being made. Furthermore, the validation does not tell us about the performance of the algorithm at time periods outside of the validation, for example, at high northern latitudes during the winter period. Corrections for the bias observed in the detection of burnt area with the low resolution instrument to burnt area estimates should be made within specified fire seasons and not applied across

a full year. Furthermore, corrections for bias should be made with consideration of the land cover distribution. Future research will work towards reducing the validation grid size. We will also undertake a comparison exercise with regional products and the MODIS global burnt area product to achieve a better understanding of the performance of these algorithms.

[13] **Acknowledgments.** We would like to thank José M. C. Pereira, Ana Barros, and João Silva for their support and Olivier Arino and colleagues at the European Space Agency (ESA) for granting the use of high resolution data sets for validation purposes.

## References

Boschetti, L., H. D. Eva, A. Brivio, and J.-M. Grégoire (2004), Lessons to be learned from the comparison of three satellite-derived biomass burning products, *Geophys. Res. Lett.*, *31*, L21501, doi:10.1029/2004GL021229.

Fuller, R. B. (1975), *Synergetics*, MacMillan, New York.

Giglio, L., G. R. van der Werf, J. T. Randerson, G. J. Collatz, and P. S. Kasibhatla (2006), Global estimation of burnt area using MODIS active fire observations, *Atmos. Chem. Phys.*, *6*, 957–974.

Jupp, T. E., C. M. Taylor, H. Balzter, and C. T. George (2006), A statistical model linking Siberian forest fire scars with early summer rainfall anomalies, *Geophys. Res. Lett.*, *33*, L14701, doi:10.1029/2006GL026679.

Patra, P. K., M. Ishizawa, S. Maksyutov, T. Nakazawa, and G. Inoue (2005), Role of biomass burning and climate anomalies for land-atmosphere carbon fluxes based on inverse modeling of atmospheric $CO_2$, *Global Biogeochem. Cycles*, *19*, GB3005, doi:10.1029/2004GB002258.

Rahman, H., and G. Dedieu (1994), SMAC: A simplified method for the atmospheric correction of satellite measurements in the solar spectrum, *Int. J. Remote Sens.*, *15*, 123–143.

Roy, D. P., Y. Jin, P. E. Lewis, and C. O. Justice (2005), Prototyping a global algorithm for systematic fire affected area mapping using MODIS time series data, *Remote Sens. Environ.*, *97*, 137–162, doi:10.1016/j.rse.2005.04.007.

Sahr, K., and D. White (1998), Discrete global grid systems, in *Computing Science and Statistics*, vol. 30, *Dimension Reduction, Computational Complexity, and Information*, edited by S. Weisberg, pp. 269–278, Interface Found. of N. Am., Fairfax Stn., Va.

Schultz, M. G. (2002), On the use of ATSR fire count data to estimate the seasonal and interannual variability of vegetation fire emissions, *Atmos. Chem. Phys.*, *2*, 387–395.

Seiler, W., and P. J. Crutzen (1980), Estimates of gross and net fluxes of carbon between the biosphere and atmosphere from biomass burning, *Clim. Change*, *2*, 207–247.

Simon, M., S. Plummer, F. Fierens, J. J. Hoelzemann, and O. Arino (2004), Burnt area detection at global scale using ATSR-2: The GLOBSCAR products and their qualification, *J. Geophys. Res.*, *109*, D14S02, doi:10.1029/2003JD003622.

Smith, R., M. Adams, S. Maier, R. Craig, A. Kristina, and I. Maling (2007), Estimating the area of stubble burning from the number of active fires detected by satellite, *Remote Sens. Environ.*, *109*, 95–106, doi:10.1016/j.rse.2006.12.011.

Stohl, A., et al. (2006), Arctic smoke record high air pollution levels in the European Arctic due to agricultural fires in eastern Europe, *Atmos. Chem. Phys. Discuss.*, *6*, 9655–9722.

Sukhinin, A. I., et al. (2004), AVHRR-based mapping of fires in Russia: New products for fire management and carbon cycle studies, *Remote Sens. Environ.*, *93*, 546–564, doi:10.1016/j.rse.2004.08.011.

Tansey, K., et al. (2004), Vegetation burning in the year 2000: Global burned area estimates from SPOT VEGETATION data, *J. Geophys. Res.*, *109*, D14S03, doi:10.1029/2003JD003598.

Turquety, S., et al. (2007), Inventory of boreal fire emissions for North America in 2004: Importance of peat burning and pyroconvective injection, *J. Geophys. Res.*, *112*, D12S03, doi:10.1029/2006JD007281.

van der Werf, G. R., J. T. Randerson, L. Giglio, G. J. Collatz, P. S. Kasibhatla, and A. F. Arellano Jr. (2006), Global estimation of burned area using MODIS active fire observations, *Atmos. Chem. Phys.*, *6*, 3423–3441.

Wotawa, G., L.-E. De Geer, A. Becker, R. D'Amours, M. Jean, R. Servranckx, and K. Ungar (2006), Inter- and intra-continental transport of radioactive cesium released by boreal forest fires, *Geophys. Res. Lett.*, *33*, L12806, doi:10.1029/2006GL026206.

E. Bartholomé and J.-M. Grégoire, Joint Research Centre, European Commission, I-21027 Ispra, Italy.

P. Defourny, J.-F. Pekel, and E. van Bogaert, ENGE Unité Environnemétrie et Géomatique, Université Catholique de Louvain, B-1348 Louvain-la-Neuve, Belgium.

R. Leigh and K. Tansey, Department of Geography, University of Leicester, Leicester, LE1 7RH, UK. (kjt7@le.ac.uk)